European Journal of Mechanics B/Fluids 49 (2015) 392–399

Contents lists available at ScienceDirect

European Journal of Mechanics B/Fluids

journal homepage: www.elsevier.com/locate/ejmflu

Global stability analysis of underexpanded screeching jets

Samir Beneddine *, Clément Mettot, Denis Sipp

Onera, The French Aerospace Lab, 8 rue des Vertugadins, 92190 Meudon, France

ARTICLE INFO

Article history:
Available online 29 May 2014

Keywords:
Screech
Stability
Global mode
Underexpanded jets

ABSTRACT

This article deals with a global stability analysis of the screech phenomenon. We have shown that a laminar underexpanded supersonic cold jet can exhibit globally unstable modes. A closer look at the structure of these modes shows that they present upstream propagating waves, which is known to be a major component of the screech phenomenon. Furthermore, we find a good agreement between the frequency of the eigenmodes and existing empirical formulas for the prediction of screech frequency. We have then studied the influence of two key parameters on the linear stability of the flow, the jet pressure ratio (JPR) and the nozzle lip thickness, which are known to play an important role in the screech phenomenon. Finally, a careful study of the structure of the unstable modes shows that the upstream propagating acoustic waves of those modes are generated by supersonic phase velocity disturbances, a well-known sound generation mechanism.

1. Introduction

The study of imperfectly expanded supersonic jets is an active subject of research since such flows can be found in a broad variety of industrial applications. The most common one is military aircrafts, whose engines often operate at off-design conditions. In this article, we focus on underexpanded jets, where the flow pressure at the nozzle exit is higher than the ambient pressure. This mismatch in pressure induces the apparition of a complex quasi-periodic "shock-cell" structure. The jet periodically overexpands and reconverges, attempting to match the ambient pressure, and consequently, forms a standing wave pattern. As a result, shocks and expansion fans appear periodically, creating the so-called shock-cells. Despite the fact that those flows are highly nonlinear, it is possible to predict the gross features of such jets, such as the shock-cell length, with a good agreement with experimental data [1–3].

One of the important features of supersonic jets is that they can generate strong noise, a point which has been intensively studied in the past decades. A large number of articles on the subject have been written since the first work of Lighthill in 1952 [4]. One may refer for instance to the review of Tam [5] for further details. It is now known that the noise of shock-containing supersonic jets has three components: the broadband shock-associated noise resulting from the interaction of instability waves and the shocks, the turbulent mixing noise generated by the turbulent fluctuations, and the screech tones, which are the subject of this article. More information about the two first noise components can be found in Tam 1995 [5].

The screech phenomenon was first studied in 1952 by Powell [6]. He observed that, under certain conditions, supersonic imperfectly expanded jets can produce very loud discrete frequency tones, the so-called screech tones. This phenomenon can be so intense that in real flight conditions, it can damage the structure of an aircraft. The first observation of such damages was made by the British Aircraft Corporation in the 1960s, where in-flight measurements showed that screech was responsible for minor cracking on VC 10 aircrafts [7,8]. Such concerns do not affect most of modern commercial engines though, and usually, screech tones are observed only with military aircrafts.

In one of his papers, Tam [5] refers to screech as "the least understood, least predictable component of supersonic jet noise". Indeed, many questions, such as the prediction of the amplitude of the noise, or its sensitivity to the surrounding environment, have remained unanswered. However, the dominant physical mechanism is known and has been described by Powell [6] as a feedback loop between the shocks and the nozzle lip: instability waves developing in the shear layer interact with the shocks, giving birth to acoustic waves propagating upstream. When those waves reach the nozzle lip, they are reflected and excite the shear layer, giving birth to new embryo perturbations that undergo the same process, closing the resonant loop.

There is abundant literature available on the topic of screeching jets: as mentioned in Raman 1999 [9], from Powell's first

* Corresponding author. Tel.: +33 634998075.
E-mail addresses: samir.beneddine@onera.fr, samir.beneddine@ens-cachan.fr (S. Beneddine).

http://dx.doi.org/10.1016/j.euromechflu.2014.05.006
0997-7546/

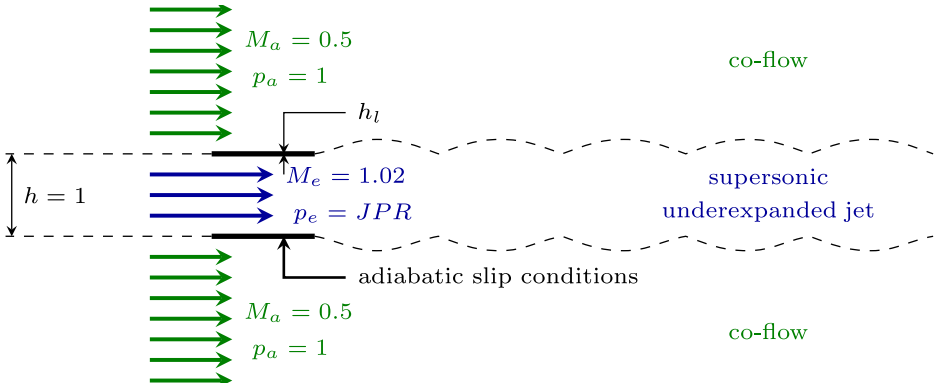

Fig. 1. Scheme of the physical configuration of the flow (nondimensional quantities). The two variable parameters are the JPR and the lip thickness h_l.

observation to now, more than 200 papers have been published. An extensive bibliography and a detailed review on screech can be found in the article of Raman [8]. But despite the large amount of studies that can be found on the topic, our knowledge of the phenomenon remains mainly qualitative. The only real quantitative prediction available is the frequency of the tones [6]. This lack of understanding is the reason screech is still an active field of research. But, to our knowledge, screech has never been studied in the light of a linear global stability analysis, which is the purpose of this article.

Recent works have shown that stability theory appears as a very successful framework for sound prediction in jets. We can cite for example the article of Lesshafft [10] on global modes in adapted subsonic hot jets, the work of Ray and Lele [11] on broadband shock-associated noise in supersonic underexpanded jets using parabolized stability equations (PSE), or Nichols [12], who performed a global mode decomposition on supersonic adapted jets. The case of screech presents one strong particularity: as briefly explained above, one of the key features of a screeching jet is that it presents upstream propagating acoustic waves that play a major role in the instability process. Consequently, a stability analysis based on PSE is unable to capture such upstream propagating structures and cannot therefore be used here. On the contrary, a global stability analysis [13,14], in which both the cross-stream and stream-wise directions of the perturbation are solved for, is able to capture upstream-propagating waves and may also handle more precisely the non-parallelism induced by the shock-cell structures. In the present article, we aim at finding an underexpanded supersonic jet that is globally unstable, and analyze the link between the unstable structures and the screech phenomenon.

The outline of the paper is as follows. After a brief reminder on global linear stability theory and on the numerical strategy adopted to perform the study, we will present an underexpanded jet configuration that is marginally unstable, and relate the features of the unstable global mode to screech. Then, we will assess the effects of two key parameters, the jet pressure ratio (JPR) and the lip thickness. In the last section, we will focus on the noise generation mechanism associated with the unstable global modes.

2. Physical configuration and linear global stability analysis

2.1. Physical configuration and governing equations

We focus on two-dimensional cold jets of air surrounded by a co-flow. In this study, the jet pressure ratio (JPR), defined as the ratio between the static jet pressure and the ambient pressure, and the lip thickness are the two parameters that will be varied. All other parameters of the configuration are fixed: the Mach number of the co-flow is 0.5, while the Mach number of the jet is 1.02. The height of the nozzle exit is equal to 3 mm. The stagnation temperature of both the jet and the co-flow is $T_0 = 288$ K, the Prandtl number is 0.72 and the viscosity follows a Sutherland law, with standard coefficients for air. The static pressure of the ambient air is set to 3000 Pa. The static pressure of the jet, and thus the Reynolds number (based on the jet velocity, the height of the nozzle, and the static density/temperature of the jet) depend on the JPR. The value of the height of the nozzle and the static pressure of the ambient air have been chosen such that, for all the studied JPR in this paper, the order of magnitude of the Reynolds number is 10^3, ensuring that the flow is in a laminar transitional situation. To simplify the study, we have imposed adiabatic slip conditions on the walls of the nozzle, so that the boundary layer thicknesses (inside and outside the nozzle) are zero at the nozzle exit: the effect of the boundary layer thickness is left for future work.

The flow dynamics is modeled using the compressible 2D Navier–Stokes equations, that can be recast in the following compact form:

$$\frac{d\mathbf{q}}{dt} = \mathcal{R}(\mathbf{q}), \tag{1}$$

where $\mathbf{q} = (\rho, \rho u, \rho v, \rho E)^T$ designates the variables describing the flow (density, streamwise momentum, cross-stream momentum, total energy) and $\mathcal{R}(\mathbf{q})$ designates the conservation of mass, momentum, and energy equations. From now on, we consider that all quantities are made nondimensional using the jet velocity, the height of the nozzle, the static pressure and density of the ambient air (see Fig. 1).

2.2. Global mode decomposition

A baseflow $\mathbf{q}_b$ is defined such that it is a stationary solution of Eq. (1). Therefore, we have $\mathcal{R}(\mathbf{q}_b) = \mathbf{0}$. If we consider a small perturbation $\mathbf{q}'$ around the baseflow, $\mathbf{q} = \mathbf{q}_b + \mathbf{q}'$, the linearization of (1) yields the following governing equation for the perturbation:

$$\frac{d\mathbf{q}'}{dt} = \mathcal{A}\mathbf{q}', \tag{2}$$

with $\mathcal{A} = \left.\frac{\partial \mathcal{R}}{\partial \mathbf{q}}\right|_{\mathbf{q}_b}$, the linearization of the operator $\mathcal{R}$ around the baseflow.

A global mode decomposition consists in finding particular solutions of (2) under the form

$$\mathbf{q}'(x, y, t) = e^{\lambda t}\hat{\mathbf{q}}(x, y), \tag{3}$$

where $\hat{\mathbf{q}}$ are the so-called global modes of the system and $\lambda = \sigma + i\omega$ is a complex scalar describing the time-behavior of the structure (σ is the amplification rate and ω the frequency of the mode). They describe the asymptotic behavior of the flow with

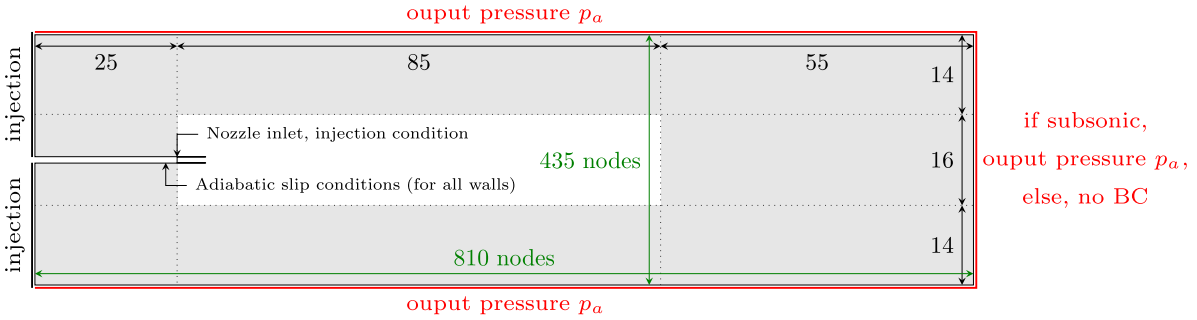

Fig. 2. Computational domain and boundary conditions. Sponge regions are in gray and the physical domain of interest is in white.

respect to small disturbances. Injecting this particular expression into (2) leads to the following eigenproblem:

$$\mathcal{A}\hat{\mathbf{q}} = \lambda\hat{\mathbf{q}}.$$

It is seen that the global modes $\hat{\mathbf{q}}$ correspond to the eigenvectors of $\mathcal{A}$, and λ to the eigenvalues. A global stability analysis consists in finding eigenvalues/eigenvectors displaying positive amplification rates.

2.3. Numerical strategy

All the computations were performed using the compressible elsA solver developed at ONERA. The spatial discretization of the governing equations is based on a second-order finite-volume conservative formulation. We use a Jameson numerical flux with scalar dissipation with Martinelli correction for the convective fluxes, and a second-order centered scheme for the diffusive fluxes.

The computational domain has 810 nodes in the streamwise direction, and 435 in the cross-stream direction, and covers an area of (165×44). Sponge regions, necessary to damp spurious reflections on the boundaries of the domain have been added. We impose respectively supersonic and subsonic injection conditions for the jet and the co-flow. Similarly to the work of Prudhomme [15], if the flow reaches the downstream boundary with a subsonic speed, we impose its pressure to be equal to the static pressure of the co-flow, if it is supersonic, no conditions are imposed. Fig. 2 shows the sponges, the physical domain of interest and the boundary conditions.

For the baseflow computations, a local time-stepping strategy is adopted, with CFL numbers equal to 30, and a time discretization based on a first order implicit Euler scheme. In any case, we checked that the explicit residuals decreased by ten orders of magnitude, to ensure the quality of the baseflow.

The stability analysis is conducted using a fully discrete approach, where the residual $\mathcal{R}$ is a vector-valued operator, and $\mathcal{A}$ corresponds to its Jacobian matrix. The extraction of the Jacobian is performed using a first-order finite difference method. Since the following approximation holds for any vector $\mathbf{u}$:

$$\mathcal{A}\mathbf{u} \approx \frac{1}{\varepsilon}\big(\mathcal{R}(\mathbf{q}_b + \varepsilon\mathbf{u}) - \mathcal{R}(\mathbf{q}_b)\big), \tag{4}$$

where ε is a small parameter, we can perform matrix–vector products with a set of well-chosen vectors to explicitly compute all non-zero coefficients of the Jacobian matrix. In order to limit the number of residual evaluations that are needed to extract the Jacobian matrix explicitly, we can optimize this choice. Relation (4) shows that when the discretization stencil of the residual $\mathcal{R}$ is compact, $\mathcal{A}$ is sparse. In this case, we can minimize the number of required residual evaluations by choosing a set of vectors $\mathbf{u}$ containing several non-zero components, far enough from each other with respect to the stencil width, in order to maximize the number of non-zero coefficients of $\mathcal{A}$ contained in $\mathcal{A}\mathbf{u}$ (see Mettot, Renac, and Sipp [16]). We choose to define the parameter ε locally, based on the local values of the components of $\mathbf{q}_b$. The accuracy of this finite-difference technique depends on the value of ε: it has to be sufficiently small with respect to the local value of the baseflow $\mathbf{q}_b$ but not too small to avoid round-off errors. We chose $\varepsilon_i = \min\big[\varepsilon_m(|q_{b_i}|+1); |q_{b_i}|/10\big]$, where q_{b_i} is the ith component of $\mathbf{q}_b$, and $\varepsilon_m = 10^{-6}$. To check the accuracy of the computation, we made sure that the same eigenvalues were obtained with Jacobian matrices based on $\varepsilon_m = 10^{-6}$ and $\varepsilon_m = 10^{-7}$.

The spectrum of $\mathcal{A}$ is then computed using a shift–invert strategy combined with Krylov methods (open-source library ARPACK [17]). Matrix inversions were carried out by the sparse direct LU parallel solver MUMPS [18]. Contrary to iterative methods, this strategy provides very fast results, the limitation being an important memory requirement.

3. Marginally unstable configuration and associated mode

3.1. Physical configuration

We consider a configuration as described in Section 2.1, with a JPR equal to 1.12 and a lip thickness $h_l = 0.063$. With those parameters, the Reynolds number is 3020.

3.2. Baseflow computation

Fig. 3 shows the computed density field. We can see the expected shock-cell structures. We have checked that this solution is spatially converged by considering meshes that are twice more dense, respectively in the streamwise and cross-stream direction. We have in particular compared the pressure distribution along the central line of the jet for the different computed fields. The maximum relative error, defined as

$$\max_{x\in[0,x_{max}]}\left(\frac{|p(x) - p_{ref}(x)|}{p_{ref}(x)}\right),$$

where p is the pressure distribution along the central line corresponding to the denser meshes, and p_{ref}, to the original mesh, is inferior to 5%.

Finally, to check the validity of our computed baseflow, we have compared the length of the computed shock-cells with Tam's formula [3]:

$$l_s = 2\frac{\sqrt{M_j^2 - 1}}{M_j}\left(\frac{1 + \frac{\gamma-1}{2}M_j^2}{1 + \frac{\gamma-1}{2}}\right)^{(\gamma+1)/2(\gamma-1)}, \tag{5}$$

where γ is the heat capacity ratio, l_s the nondimensional length of the shock-cells, and M_j, the fully expanded Mach number, defined as (see Berland et al. [19]):

$$M_j = \sqrt{\frac{2}{\gamma-1}\left[\left(1 + \frac{\gamma-1}{2}M_e^2\right)\mathrm{JPR}^{(\gamma-1)/\gamma} - 1\right]}. \tag{6}$$

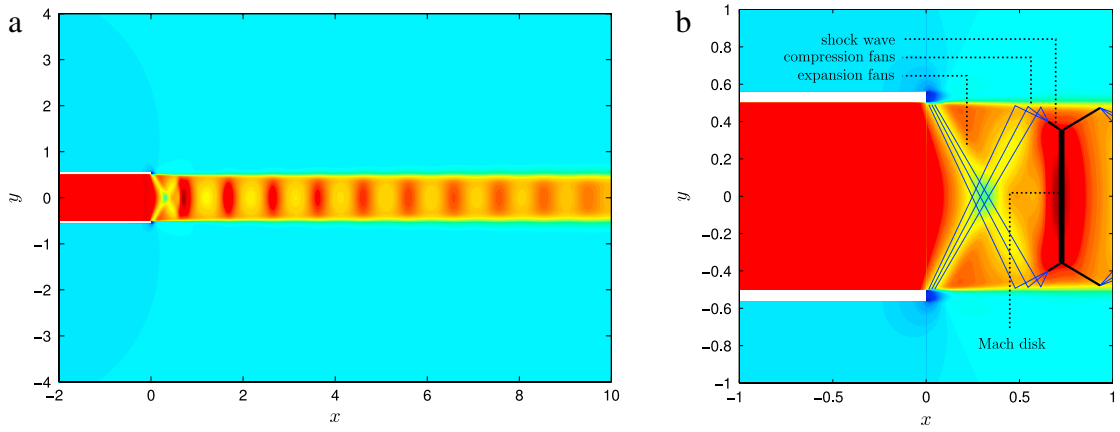

Fig. 3. (a) Density field of the computed baseflow (JPR $= 1.12$, $h_l = 0.063$). One can notice the expected shock-cell structure. (b) Zoom on the exit of the nozzle, on which we have represented the main features of underexpanded jets.

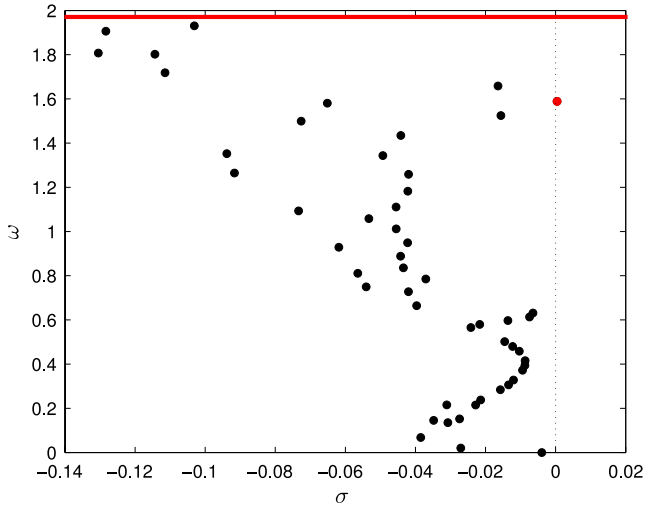

Fig. 4. Spectrum of the Jacobian matrix, for the marginally unstable configuration (JPR $= 1.12$, $h_l = 0.063$). Red dot: the marginally unstable eigenvalue, red line: frequency prediction (Powell's formula [6]).

For the studied configuration, the formula gives $l_s = 0.99$. Using the computed baseflow, we can measure the length of the cells, for instance by evaluating the distance between two local pressure maxima along the centerline of the jet. Table 1 shows that the results are in very good agreement with Eq. (5).

3.3. Global mode decomposition

Fig. 4 shows the least stable eigenvalues corresponding to the baseflow presented in the above section. We can see that there exists one marginally unstable global mode and a series of damped global modes.

Fig. 5 shows the spatial structure of the marginal global mode. One can clearly notice that the density field presents upstream propagating waves in accordance with the screech phenomenon (a video of the temporal behavior of the mode has been provided as supplementary material (see Appendix A) for better visualization of its spatial structure). We can observe that the radiated sound field is out-of-phase on either side of the jet, in accordance with most of the works carried out on rectangular and planar jets (see the review of Raman [8]). However, it has also been shown that rectangular jets can sustain a weak symmetric mode [8,20], but several papers suggest that, in the strictly two-dimensional case, this mode should not appear [20,21].

Table 1
Comparison between the measured shock-cell lengths from the computed baseflow (for the five first shock-cells) and the theoretical values $l_s = 0.99$ (Eq. (5)), for the case JPR $= 1.12$, $h_l = 0.063$.

Shock-cell no.	1	2	3	4	5
Shock-cell length (comp. baseflow)	0.960	0.978	0.983	0.978	0.995
Relative error (w.r.t. formula (5))	3.0%	1.3%	0.7%	1.3%	0.5%

To confirm that this mode is indeed related to screech tones, we have compared its frequency with empirical formulas. Powell [6] provides a simple formula to predict the frequency of the tones, given by

$$f = \frac{u_c}{l_s(1 + u_c/c_a)}, \tag{7}$$

where f is the frequency, l_s the length of the shock-cells, u_c the convective speed of the disturbance, and c_a the ambient sound velocity. This formula indicates that one period of screech corresponds to the sum of the time needed for a disturbance to reach the first shock ($t_1 = l_s/u_c$) and the time needed for the generated acoustic waves to travel back from this shock to the nozzle lip ($t_2 = l_s/c_a$). This leads to a period for each screech cycle equal to $T = t_1 + t_2 = l_s(u_c + c_a)/(u_c c_a)$, from which one can easily deduce Powell's formula. The convective velocity u_c is generally taken equal to $a \cdot u_j$, with u_j the jet velocity, and a a scalar around 0.5–0.7 [8]. Eq. (7) holds when the ambient air is at rest. In our case,

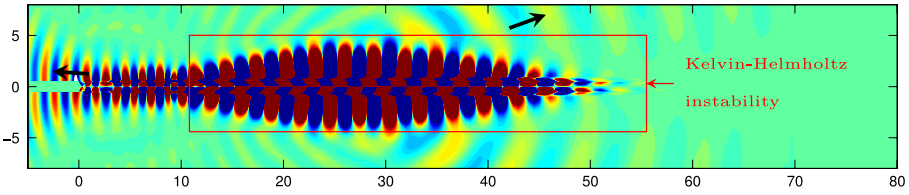

Fig. 5. Real part of the density field of the marginally unstable mode (JPR $= 1.12$, $h_l = 0.063$). One can notice the upstream propagating waves, typical from screech. The structures in the red rectangle propagate downstream. The black arrows show the direction of propagation of the acoustic waves.

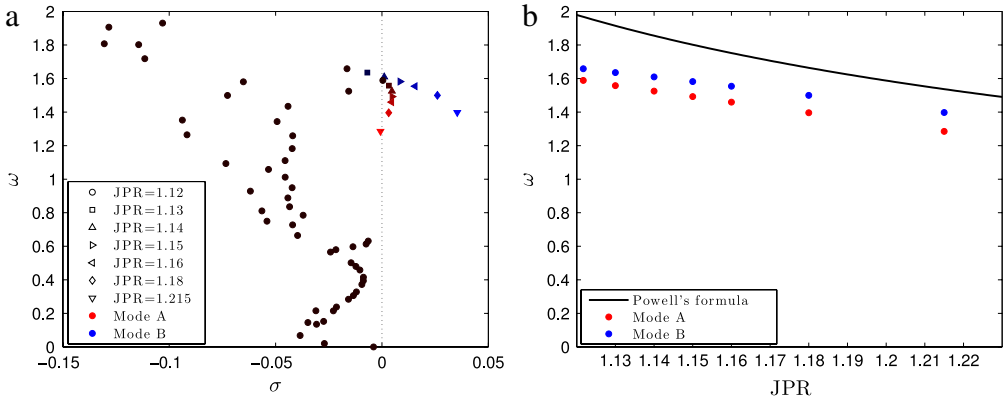

Fig. 6. (a) Spectrum of the JPR = 1.12 configuration (circles), with the evolution of mode A (red) and B (blue) when we increase the JPR, $h_l = 0.063$. Brighter colors correspond to higher JPRs. (b) Comparison between the analytically derived evolution of the frequency with respect to the JPR (based on Eq. (8), using Eq. (6) and (5)), and the frequencies of mode A and B. (For interpretation of the references to color in this figure legend, the reader is referred to the web version of this article.)

since we have a co-flow, the convection speed of the perturbation needs to be modified according to:

$$u_c = a(u_j - u_a) + u_a,$$

where u_a is the ambient velocity. The acoustic feedback is also impacted by the co-flow, and sound waves propagate back to the nozzle with a speed equal to $c_a - u_a$ instead of c_a. This yields the following final relation for the frequency prediction:

$$f = \big(a(u_j - u_a) + u_a\big)\left(l_s\left[1 + \frac{a(u_j - u_a) + u_a}{c_a - u_a}\right]\right)^{-1}. \tag{8}$$

In the present case, this formula yields $\omega = 2\pi f \approx 1.96$. We can see that the frequency of the unstable mode is in reasonable agreement with this value (18 % of error, see Fig. 4). The discrepancy could stem from the fact that global stability analysis performed around baseflows may provide frequencies that are different from those observed on saturated limit-cycles (see for instance [22]). We can also point out that predictions based on (7) overestimate frequencies for low values of M_j (and thus, low values of JPR) with respect to experimental data (see for example [8]), in agreement with the present results. Therefore, we expect better consistency between the global mode frequency and Eq. (8) for higher values of JPR (see next section). But those first results show that both the structure of the mode and its frequency support the idea that screech is linked to a global instability of the jet.

4. Influence of the jet pressure ratio

The influence of the JPR on the screech phenomenon is still an open question, in particular there is no simple relation between the JPR and the intensity of the tones [8]. Yet, we know that this parameter plays a major role in the phenomenon since it has a strong influence on the length of the shock-cells l_s and on the convective velocity u_c. An increase of the JPR leads to a larger value of M_j, and therefore larger values of u_c and l_s (see Eq. (5)), the resulting effect being a decrease of the frequency.

4.1. Physical configurations

To assess the effect of the JPR parameter on the eigenvalues, we consider seven configurations with a fixed value of the lip thickness $h_l = 0.063$ but with JPR values ranging from 1.12 to 1.215, and compute the associated spectrum. The studied values of JPR and the corresponding Reynolds numbers are reported in Table 2.

Table 2
Studied values of JPR and corresponding Reynolds numbers ($h_l = 0.063$).

JPR	1.12	1.13	1.14	1.15	1.16	1.18	1.215
Re	3020	3050	3070	3100	3120	3170	3270

4.2. Results

We have reported in Fig. 6 the full spectrum for JPR = 1.12 (circular symbols) and the unstable eigenvalues for higher values of the JPR (other symbols). We can see that there are two families of unstable modes (red and blue symbols), that will respectively be called modes A and B in the following. The marginal global mode described in the previous section is an A-mode. The spatial structure of the new unstable mode (mode B) can be seen in Fig. 7. Similarly to mode A, it exhibits upstream propagating waves in accordance with the screech phenomenon. The two modes exhibit a frequency decreasing when the JPR increases, confirming their link with the screech phenomenon. From Fig. 6(b), we observe that the two modes display a frequency in much closer agreement with Powell's formula as the JPR is increased.

One last point about those results can be commented: the growth rate, for which we have no theoretical results, presents an interesting behavior. Indeed, we can observe that mode A, the first to become unstable, stabilizes again when we increase the JPR, while the other mode has, within the studied range of JPRs, a simpler behavior, with a growth rate increasing when the JPR becomes higher. This shows us that mode A is unstable only for a very narrow range of JPRs, meaning that mode B is certainly more relevant for the study of screech, which is known to be a phenomenon occurring for a wider range of JPRs.

5. Influence of the nozzle lip thickness

The lip thickness is another parameter known to have a major influence on screech tones. As mentioned before, the mechanism of generation of the tones is based on a resonant feedback loop with upstream propagating acoustic waves that are reflected on the lip and excite the mixing layer. The thicker the lip is, the larger the reflecting surface is. The experiment of Ponton and Seiner [23] reported that increasing the nozzle lip thickness tends to significantly increase screech tone amplitudes. Also, we know that screech ceases to exist when the fully expanded Mach number M_j is large enough [8], but it appears that even in such non-screeching jets, it can be reactivated by adding a thickener on the lip [24]. The frequency is also slightly affected by this parameter, and tends to increase when h_l is larger, as it has been shown for instance by Kim [25]. But, to our knowledge, there is no prediction formula accounting for this parameter. The influence of the lip thickness is still one of the points that is not entirely understood in the screech phenomenon.

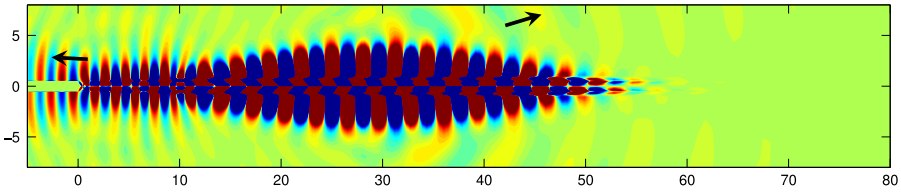

Fig. 7. Real part of the density field of mode B (JPR = 1.18, $h_l = 0.063$). One can notice the upstream propagating waves, typical of screech, similar to what can be seen in the other mode (Fig. 5). The black arrows show the direction of propagation of the acoustic waves.

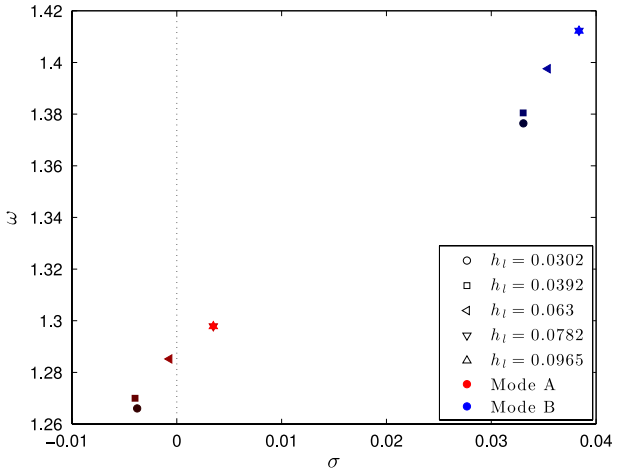

Fig. 8. Eigenvalues of mode A (red) and B (blue) for different nozzle lip thicknesses h_l (JPR = 1.215). Lighter colors correspond to higher thicknesses. Remark: the eigenvalues corresponding to the two higher lip thicknesses are very close, making hard to distinguish one from the other. (For interpretation of the references to color in this figure legend, the reader is referred to the web version of this article.)

Table 3
Values of lip thickness that have been considered for the parametric study (JPR = 1.215).

h_l	0.0302	0.0392	0.0630	0.0728	0.0965

5.1. Physical configurations

To study the impact of the lip thickness on the global stability, we consider five different lip thicknesses (see Table 3), with a fixed value of the JPR = 1.215 (Re = 3270).

5.2. Results

Fig. 8 shows the evolution of the eigenvalues corresponding to mode A and mode B. Mode A is stable for the three thinner lips, but is unstable with the two thicker lips. A similar behavior is observed in mode B, which has a growth rate increasing when h_l becomes larger. As expected, the thicker the lip is, the more unstable the modes are. The frequency is also slightly altered and becomes higher for thicker lips, in agreement with the paper of Kim [25] who pointed out that an increase of lip thickness causes a decrease in screech wavelength and therefore an increase of the frequency. One can also notice that the spectrum displays a saturation-like behavior: we can see that both the frequency and the growth rate are practically not altered when we compare the two smaller or the two larger thicknesses. This behavior is reminiscent of the experiments led by Raman [8], where the strength of the oscillations of the jet increases when the lip becomes thicker, until a certain point beyond which no appreciable change is seen anymore.

6. Noise generation mechanism

We have identified two unstable modes related to screech, and we have observed that they exhibit upstream propagating acoustic waves. Here, we focus on the sound generation mechanism responsible for the birth of those waves.

One of the well-known mechanism of sound generation is the presence of supersonic phase velocity disturbances [5]. Global stability analysis provides the temporal and spatial linear behavior of the conservative variables of modes A and B. We have then computed the associated vorticity field for each mode, using a second-order centered scheme for spatial derivations of the velocity (see Fig. 9). Then, the local streamwise phase velocity of the resulting field is given by:

$$v_\phi^x = -\frac{\omega}{\partial \boldsymbol{\phi}/\partial x}, \quad \text{with } \boldsymbol{\phi} = arg(\hat{\boldsymbol{\omega}}), \tag{9}$$

where $\hat{\boldsymbol{\omega}}$ is the complex vorticity field of the mode. We consider the case JPR = 1.18 and h_l = 0.063. As seen in Fig. 10, for the two modes, there exist streamwise locations where v_ϕ^x is higher than the ambient sound velocity c_a, confirming that the sound generation is caused by the supersonic phase velocity mechanism. Both modes display evenly distributed supersonic phase velocity locations. Such observation is reminiscent of the work of Panda et al. [26], where the convective velocity of coherent fluctuations inside the shear layer, measured experimentally, presented such a feature. One can see in the video showing the vorticity of the modes (provided as supplementary material (see Appendix A) of this article) that those regions correspond indeed to locations where the structures accelerate abruptly.

As a remark, we want to point out that Eq. (9) is meaningless where the vorticity is too small or equal to zero. Indeed, the computed vorticity values need to be significantly greater than machine precision or numerical errors due to the finite difference scheme used to compute vorticity. The computed phase velocity has no physical meaning in low-vorticity areas. Therefore, for both modes, Fig. 10 shows the phase velocity only where we have ensured that vorticity is high enough.

7. Concluding remarks

The screech phenomenon has been studied through a linear global stability analysis. We have seen that, under certain circumstances, underexpanded cold jets can be globally unstable. The associated unstable modes have a structure reminiscent of the screech phenomenon. In particular, they all present upstream propagating acoustic waves, whose frequency is in good agreement with empirical prediction formulas such as Powell's formula [6]. We have performed a parametric study on two parameters, the JPR and the lip thickness, and the behavior of the frequency of the unstable modes is consistent with Powell's formula. We have also been able to identify the sound generation mechanism of the modes: we have seen that all the modes contain supersonic phase velocity disturbances, which is a mechanism that has already been

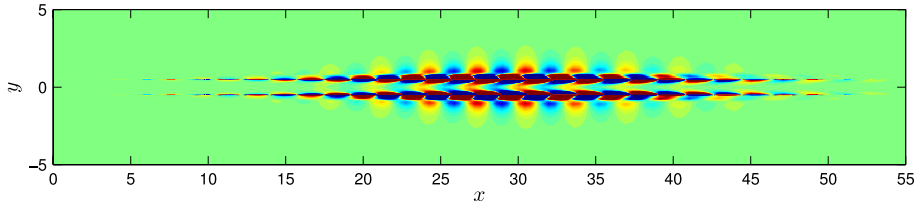

(a) Mode A.

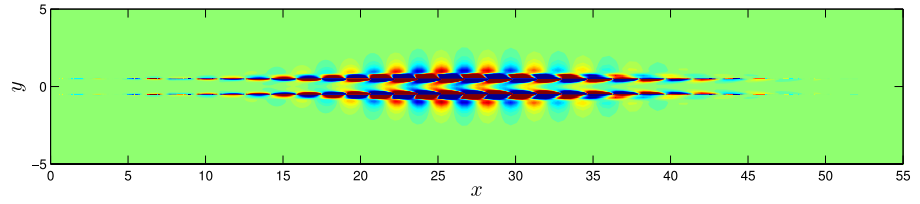

(b) Mode B.

Fig. 9. Real part of the vorticity field of the two unstable modes (JPR $= 1.18$, $h_l = 0.063$).

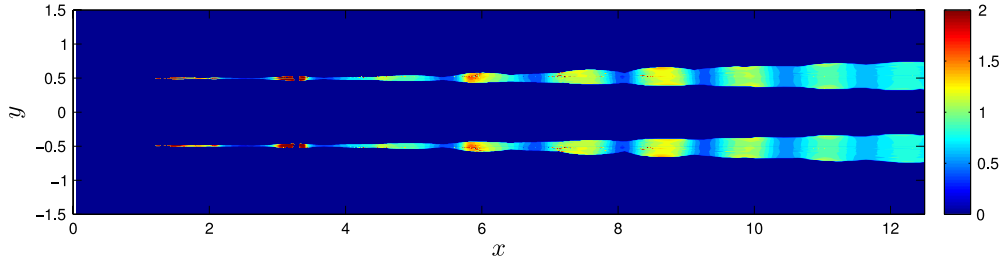

(a) Mode A.

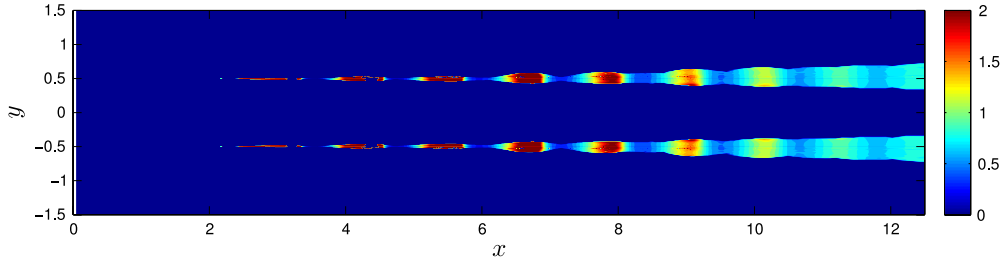

(b) Mode B.

Fig. 10. Colormap of the quantity v_ϕ^x/c_a, with v_ϕ^x as the local phase velocity of the vorticity field, and $c_a = 1.04$ the ambient sound velocity, for the case JPR $= 1.18$, $h_l = 0.063$. Only regions where vorticity is high enough with respect to numerical errors are shown.

reported as playing a role in screech tones in previous papers [5]. All those points show us that screech is indeed the result of a global instability of the flow.

This study offers a new viewpoint on the problem of screech tones. In particular, in aircraft design, where screech is something that should be avoided, the fact that it can be described as a global instability opens new possibilities for future works. For instance, the problem of screech suppression has been intensively studied during the past decades (see Norum 1983 [27] or more recently the article of Ramakrishnan [28]). For this topic, we could for example perform a sensitivity analysis of the global mode's amplification rate to see how and where we need to act in order to reduce, and maybe suppress the instability.

Appendix A. Supplementary material

Supplementary material related to this article can be found online at http://dx.doi.org/10.1016/j.euromechflu.2014.05.006.

References

[1] L. Prandtl, Stationary waves in a gaseous jet, Phys. Z. 5 (1904) 599–601.
[2] D. Pack, A note on Prandtl's formula for the wave-length of a supersonic gas jet, Quart. J. Mech. Appl. Math. 3 (2) (1950) 173–181.
[3] C. Tam, The shock-cell structures and screech tone frequencies of rectangular and non-axisymmetric supersonic jets, J. Sound Vib. 121 (1) (1988) 135–147.
[4] M. J. Lighthill, On sound generated aerodynamically. i. General theory, Proc. R. Soc. Lond. Ser. A. Math. Phys. Sci. 211 (1107) (1952) 564–587.
[5] C. K. Tam, Jet noise: since 1952, Theoret. Comput. Fluid Dyn. 10 (1–4) (1998) 393–405.
[6] A. Powell, On the mechanism of choked jet noise, Proc. Phys. B 66 (12) (1953) 1039.
[7] J. Hay, E. Rose, In-flight shock cell noise, J. Sound Vib. 11 (4) (1970) 411–420.
[8] G. Raman, Advances in understanding supersonic jet screech: review and perspective, Progr. Aerosp. Sci. 34 (1–2) (1998) 45–106.
[9] G. Raman, Supersonic jet screech: half-century from powell to the present, J. Sound Vib. 225 (3) (1999) 543–571.
[10] L. Lesshafft, P. Huerre, P. Sagaut, Aerodynamic sound generation by global modes in hot jets, J. Fluid Mech. 647 (1) (2010) 473–489.
[11] P. K. Ray, S. K. Lele, Sound generated by instability wave/shock-cell interaction in supersonic jets, J. Fluid Mech. 587 (1) (2007) 173–215.

[12] J. Nichols, S. Lele, P. Moin, Global Mode Decomposition of Supersonic Jet Noise, Center for Turbulence Research Annual Research Briefs, Stanford, CA, 2009.
[13] D. Sipp, O. Marquet, P. Meliga, A. Barbagallo, Dynamics and control of global instabilities in open-flows: a linearized approach, Appl. Mech. Rev. 63 (3) (2010) 030801.
[14] V. Theofilis, Global linear instability, Annu. Rev. Fluid Mech. 43 (2011) 319–352.
[15] S. Prudhomme, H. Haj-Hariri, Investigation of supersonic underexpanded jets using adaptive unstructured finite elements, Finite Elem. Anal. Des. 17 (1) (1994) 21–40.
[16] C. Mettot, F. Renac, D. Sipp, Computation of eigenvalue sensitivity to baseflow modifcations in a discrete framework: application to open-loop control, J. Comput. Phys. 269 (0) (2014) 234–258.
[17] R. R. B. Lehoucq, D. D. C. Sorensen, C.-C. Yang, Arpack User's Guide: Solution of Large-Scale Eigenvalue Problems With Implicityly Restorted Arnoldi Methods, vol. 6, Siam, 1998.
[18] MUMPS: a MUltifrontal Massively Parallel sparse direct Solver, http://graal.ens-lyon.fr/MUMPS/.
[19] J. Berland, C. Bogey, C. Bailly, Numerical study of screech generation in a planar supersonic jet, Phys. Fluids 19 (7) (2007) 075105.
[20] D. Lin, A. Powell, Symmetrical oscillation modes in choked-jet edge tones and screech from rectangular nozzles, J. Acoust. Soc. Am. 102 (2) (1997) 1235–1238.
[21] Y. Umeda, R. Ishii, T. Matsuda, A. Yasuda, E. Shima, et al., Instability of astrophysical jets. ii numerical simulation of two-dimensional choked underexpanded slab jets, Progr. Theoret. Phys. 84 (5) (1990) 856–866.
[22] D. Sipp, A. Lebedev, Global stability of base and mean flows: a general approach and its applications to cylinder and open cavity flows, J. Fluid Mech. 593 (2007) 333–358.
[23] M. Ponton, J. Seiner, The effects of nozzle exit lip thickness on plume resonance, J. Sound Vib. 154 (3) (1992) 531–549.
[24] G. Raman, Cessation of screech in underexpanded jets, J. Fluid Mech. 336 (1997) (1997) 69–90.
[25] Y. Kim, D. J. Lee, Acoustic properties associated with nozzle lip thickness in screeching jets, J. Mech. Sci. Technol. 21 (5) (2007) 764–771.
[26] J. Panda, An experimental investigation of screech noise generation, J. Fluid Mech. 378 (1999) 71–96.
[27] T. Norum, Screech suppression in supersonic jets, AIAA J. 21 (2) (1983) 235–240.
[28] R. Ramakrishnan, S. Raimondo, A. Grewal, G. Elfstrom, Screech suppression of supersonic jet noise, Canad. Acoust. 37 (3) (2009) 86–87.